

Methodology

The methodology of the thesis is subdivided into Geometric, Aerodynamic and Structural Models followed by the FSI Scheme used.

1.1. Geometric Model

For this FSI study, the NASA Common Research Model (CRM) will be used. It is a representative model of a common transonic aircraft that is present today, particularly a Boeing 777-200. Vasseberg et al. [1] developed this model in 2008 for setting benchmark results for future aircraft development and research on upcoming iterations of the design.

This thesis will focus on the wing only, excluding the horizontal, vertical tail and the fuselage as the main focus is on the wing responses and motions. It is assumed, the inclusion of other surfaces of the aircraft will not have any major impact to the responses of the wing, if so, it will be very minimal. This model has been studied extensively by numerous authors for its aerodynamic, structure and aeroelastic behaviours, through wind tunnel experiments and computational methods as well.

An important point to note with the current CRM wing model is the fact that it was purpose built for aerodynamic analysis. This implies the wing is already deformed into the shape as it would ideally be in flight, so called "*1-g shape*". Given the aeroelastic nature of the research objective, we require a baseline undeformed shape of the CRM wing, a so called "*jig shape*", which deforms due to forces exerted by the flow.

Brooks et al.[2] introduced the uCRM to enhance its functionality for aeroelastic analysis. The uCRM features an undeflected wing that allows for in-depth exploration of the interaction between aerodynamics and structural dynamics. Due to the research objective, the uCRM is chosen as the benchmark model and will be used as a basis for developing the geometrical model.



Figure 1.1: CAD Model of the CRM9 Wing Jig Shape[2]

1.1.1. Modelling the Minitab Wing

The process of modelling the minitab over the uCRM9 wing was done with 2 key factors in check. One was to keep the modifications to literature backed and sourced models to a minimum, since it allows easy replication and ease in implementing updates for various future iterations and cases. Secondly, the actual methodology of modelling these minitabs should be computationally efficient and interference with geometric and mesh quality should be minimum.

To model the minitab surface in CAD, 'Ruled Surfaces' Tool on SolidWorks was used. Ruled surfaces allow the creation of surfaces that extend from edges in a specified direction [3]. This allows a surface to be created normal to the curvature of the underlying model.

The complete step-by-step procedure to model the minitab surfaces can be viewed in Section A.1.

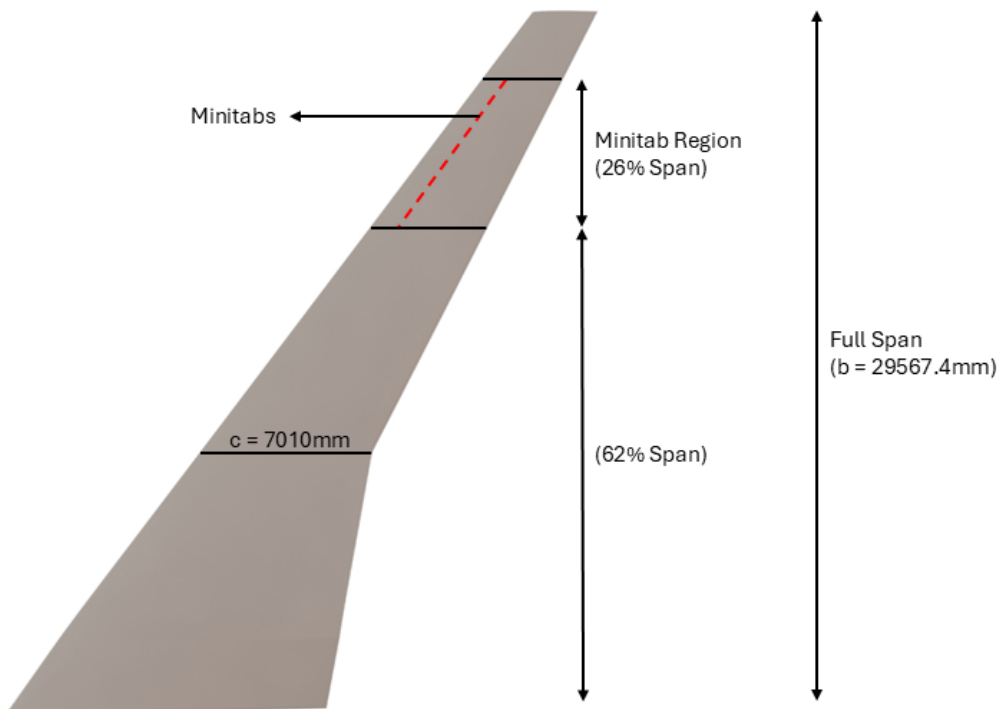


Figure 1.2: Minitab Geometry and Position

The minitabs are modelled as a permanent addition to the baseline uCRM9 wing design. The actuation and motion of the ASVG to switch from the VG to minitab was not modelled due to time and computational constraints. As stated previously, the minitab configuration will be simulated with the actuation modelled through an ON/OFF switchable condition.

The main reference model for the FSI study as seen in Figure 1.2, has 1 particular configuration of the minitab setup, with design parameters listed in Table 1.1.

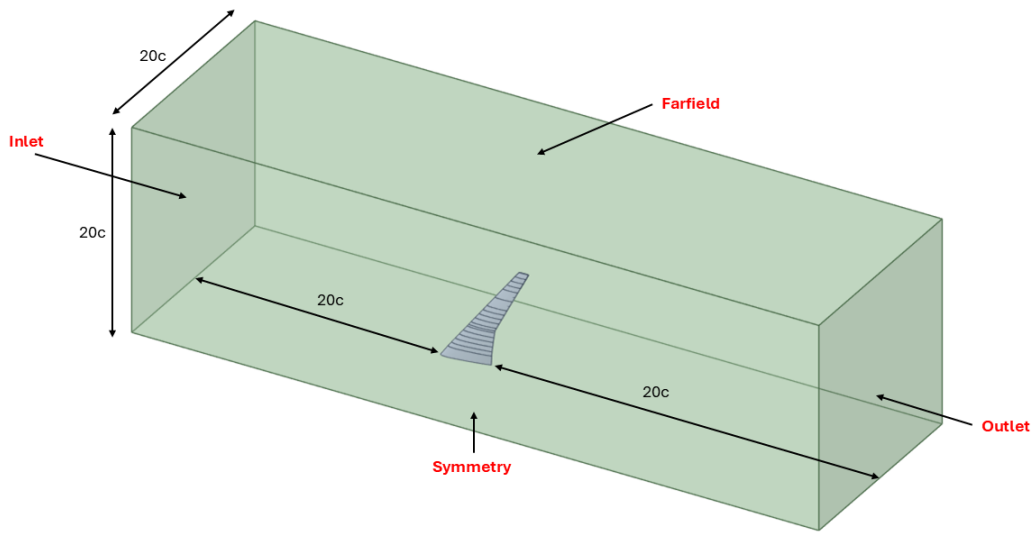
1.2. Aerodynamic Model

This section will explain the CFD domain modelled, including details about mesh generation. Finally, the setup of the CFD solver is addressed.

Table 1.1: Minitab Design Parameters

Parameter	Value
Height	75mm ($h/c = 1.07\%$)
Wall Ratio	0.4
Covering Span Length	9410mm ($y/b = [0.62 - 0.88]$)
Aspect Ratio	2

1.2.1. CFD Domain and Setup

**Figure 1.3:** Fluid Domain Model

The CFD domain consists of the uCRM9 wing, in a rectangular fluid domain. Each surface of the fluid domain is kept 20 chord lengths away from the wing, in order to avoid any undesirable influence of the boundaries.

The speed regime of the flow is transonic flow, hence compressibility of the fluid must be accounted for, which means the density and viscosity of the fluid cannot be kept constant. The density is set to follow the "*Ideal Gas Law*" and viscosity set to follow "*Sutherland's law*". The wing is set to be simulated in cruise conditions at an altitude of 11000m, giving a decreased operating pressure of 22000Pa, temperature of 215K and a density of 0.35kg/m^3 .

Boundary conditions set for the various surfaces in the CFD Domain are listed in Table 1.2:

1.2.2. Mesh Generation

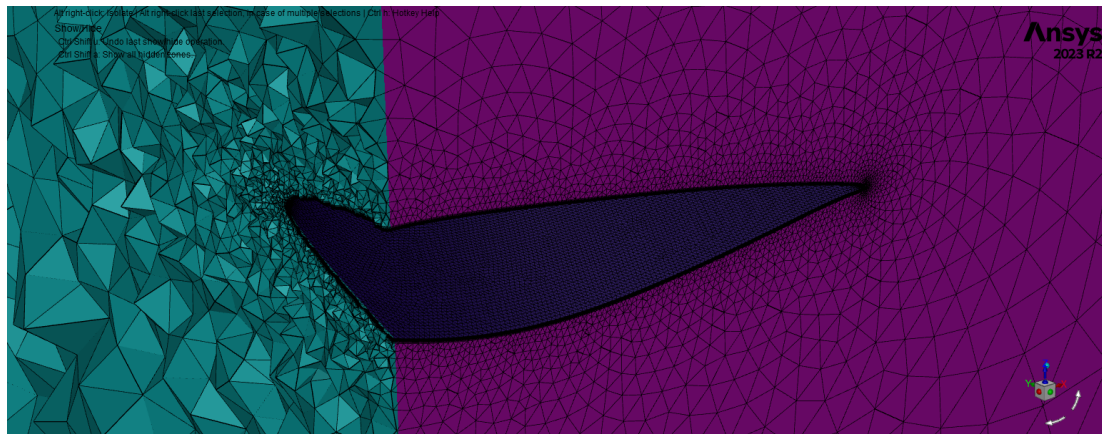
The volume mesh with mesh parameters as seen in Table 1.3 is displayed in Figure 1.4

Table 1.2: Boundary Conditions

Surface Name	Boundary Condition Type
Inlet	Pressure-Far-Field ($M = 0.85$) ; AOA = 0°
Outlet	Pressure-Far-Field ($M = 0.85$) ; AOA = 0°
Farfield	Pressure-Far-Field ($M = 0.85$) ; AOA = 0°
Symmetry	Symmetrical Boundary
Wing	Wall
Minitab	Interior to Wall (Switch)

Table 1.3: Mesh Size Parameters (100% Element Size)

Parameter	Value
Wing Surface Mesh Max Size	250mm
General Surface Size	250mm - 25000mm
Volume Element Type	Tetrahedral
Volume Element Max Size	32084mm
Total Cell Count	7149991

**Figure 1.4:** Volumetric Mesh of Fluid Domain

The minitab modelled as a surface, requires the mesh to be conformal on both sides of the minitab for higher accuracy. This ensures that the forces and flow around the minitab is transferred across the minitab without any interpolation error.

To capture the gradients and flow near the minitab, the boundary layer mesh itself, is extended upto the height of the minitab. The prismatic layer of cells with very high aspect ratio, captures the intricate flow details around the minitab.

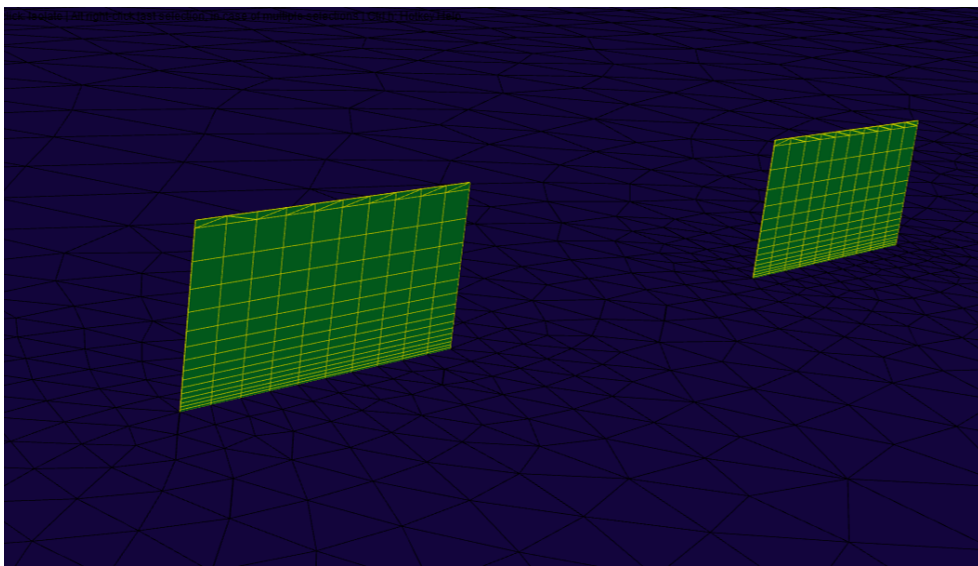


Figure 1.5: Prismatic Mesh around minitab

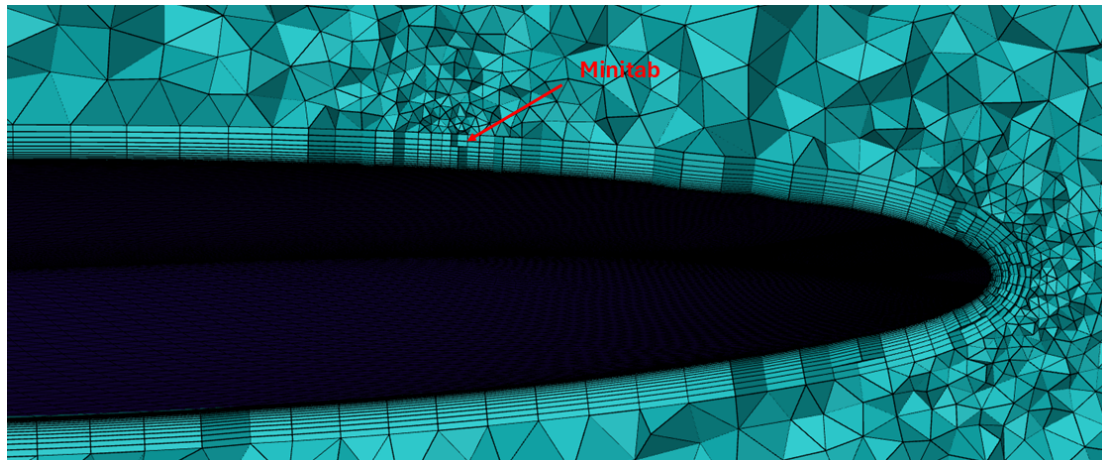


Figure 1.6: Volumetric Mesh around minitab

1.3. Structural Model

Two versions of the structural model are taken for this thesis. The Static FSI was conducted with a complete wingbox FEM model. Due to the computational resources and time required for Dynamic FSI simulations, the FEM model is reduced to a beam model.

1.3.1. Wingbox FEM model

For this thesis, the structural model used in this project was provided by the Technical University of Delft which is an in-house developed CRM structural model based on the undeflected CRM structure previously presented by Brooks et al.[2].

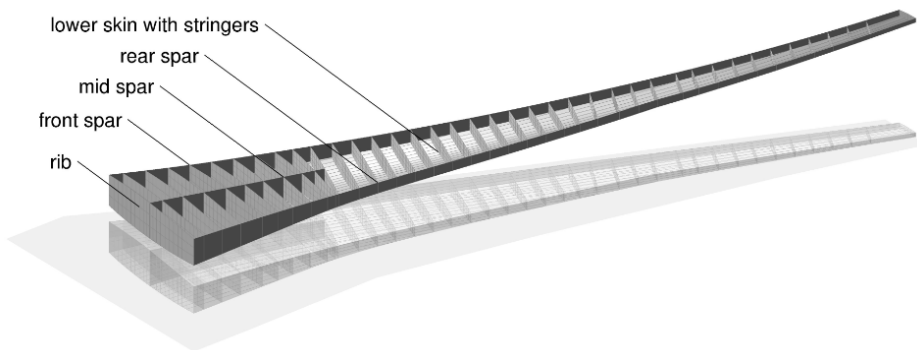


Figure 1.7: Example design of the internal wing structure without the skin

1.3.2. Beam Model

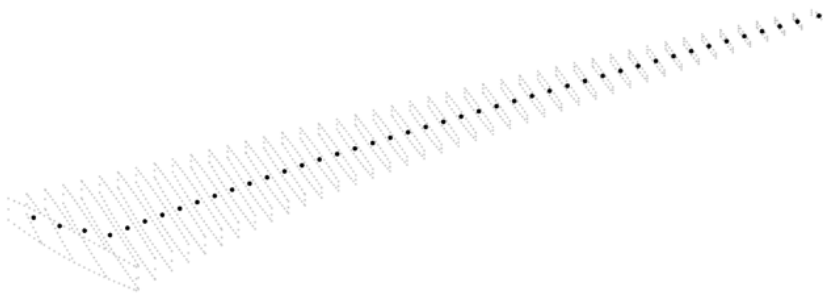


Figure 1.8: Beam Model[4]

In order to reduce the model from the full wingbox to a beam element model, the nodes at the centroid of each of the 44 ribs in the FEM wingbox model were taken to be the beam model. A generalized mass-spring-damping equation is used to calculate the displacement, velocity and acceleration of each of the nodes, subjected to the external aerodynamic loads.

(1.0)

NASTRAN offers a "*Model Reduction and Superelements*" process to take in a finite element model, and split it into interior and exterior nodes. The FEM of the component is then mathematically reduced to just the interior nodes, before assembling it into a model of the system. By providing the complete wingbox structure, NASTRAN converts this model into a reduced beam element model and the corresponding mass and stiffness elements are exported as a "pch" punchfile using the (DMIGPCH) command.

Damping Coefficient Calculation

Calculation of the damping coefficient values of a structure is not very intuitive, and typically requires experimental setups such as modal analysis, ground vibration tests (GVT), to determine the damping coefficient values[5].

Details on the various test cases and the results can be viewed in the Appendix Section A.2. As a result from this study, a Rayleigh Damping Coefficient value of 5% (K) was chosen for all the dynamic FSI simulations.

1.4. FSI Scheme

In order to study aeroelastic behaviour, it will involve the synergy between the structure and the aerodynamics, in terms of loads and displacements. The structural and aerodynamic simulations are going to be handled separately on different solvers, and hence would need to be able to communicate with each other.

1.4.1. Static FSI Algorithm

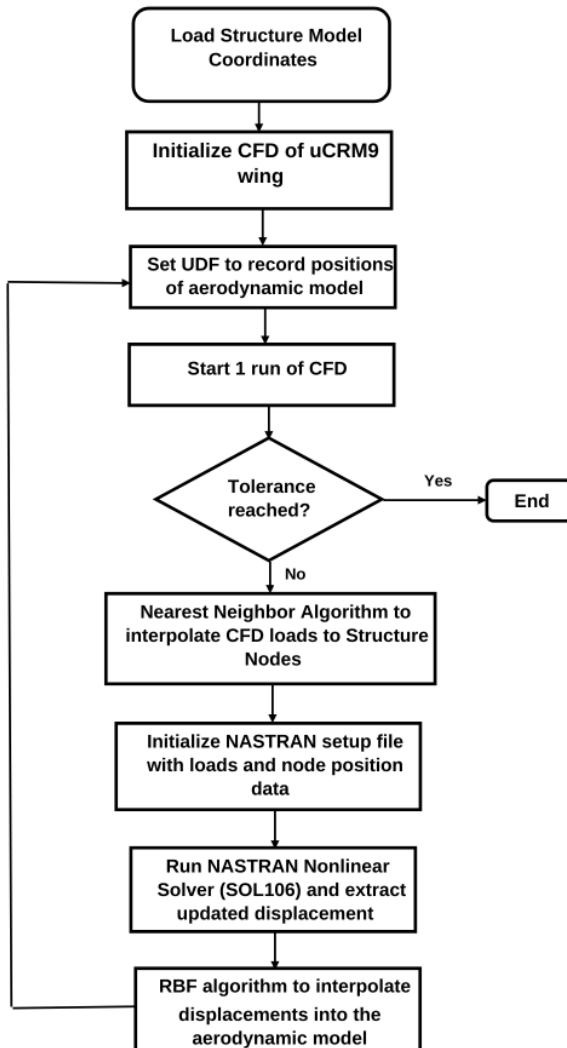


Figure 1.9: Static FSI Flowchart

1.4.2. Dynamic FSI Algorithm

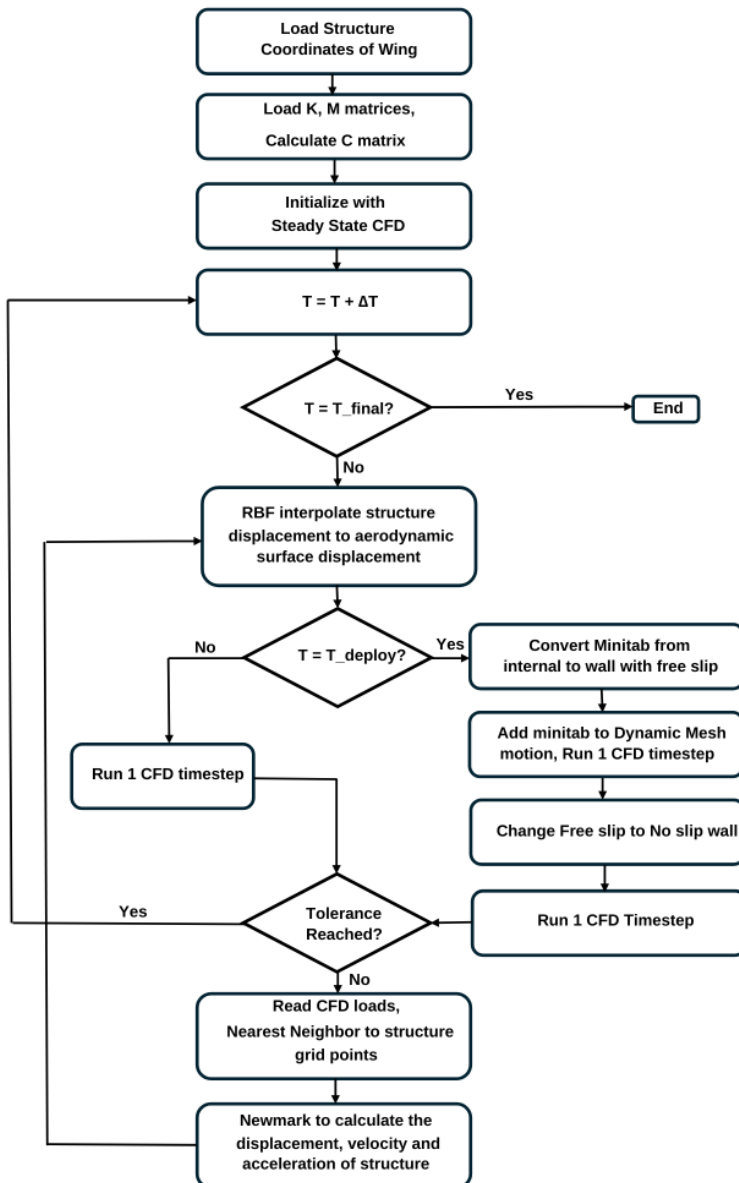


Figure 1.10: Dynamic FSI Flowchart for Minitab Deployment

In order to include the mid flight deployment of the minitab, certain modifications to the FSI framework code had to be made to simulate actuation of the minitab. A sudden inclusion of the minitab into a clean transonic simulation results in instability in the simulation and eventually diverges. The key reason for its instability is the "no-slip" setting for a wall boundary condition in Fluent. The sudden deceleration of the flow on the minitab surface is difficult for the CFD solver to model, even with small physical time step sizes.

In order to stabilize the simulation at the point of deployment, the minitab surface is converted into wall, with a free slip condition. Free Slip walls slows the flow normal to the surface to 0, but flow tangential to the surface is free, with no boundary layer formed.

This "free-slip" boundary condition was set to run for 1 time-step, to allow the flow to develop around

the minitab, slipping past the minitab and not develop any boundary layer. After convergence of the CFD and FSI solution, the minitab surface is changed to a "no-slip" wall. The previous free slip wall allows the change to the no slip wall to be less abrupt, and with the help of under relaxation factors, the solution continue to iterate without any stability issues. The whole process is reversed to simulate the "**Stow Minitab**" operation.

2

Static FSI Results for Minitab Wing

This chapter will show the results of the static FSI for the CRM wing in the Clean and Minitab configurations.

A key point to note here is that the complete wingbox model is used as the structural model for the FSI simulation as seen in Figure 1.7. Later on, the dynamic FSI case will simplify the wingbox model into a reduced multi node beam model.

2.1. Comparative Analysis of Clean and Minitab Wing

Boundary Conditions of the computational domain were set in accordance to typical cruise conditions for a passenger aircraft. Details regarding the type of boundary condition and values can be seen in Table 1.2. The two wing configurations were initialized at a cruising altitude of 11000m. Using the Altitude-temperature correlation and a constant temperature of 215K (-58°C), air density of 0.35kg/m^3 and a velocity of 249.75m/s which corresponds to a mach number ($M=0.85$) are set as the initial boundary conditions.

Table 2.1: Static FSI Results

Wing Configuration	Lift Coefficient (CL)	Drag Coefficient (CD)	Tip Displacement
Clean Wing	0.389	0.017	1288.68mm
Minitab Wing	0.364	0.021	1161.97mm

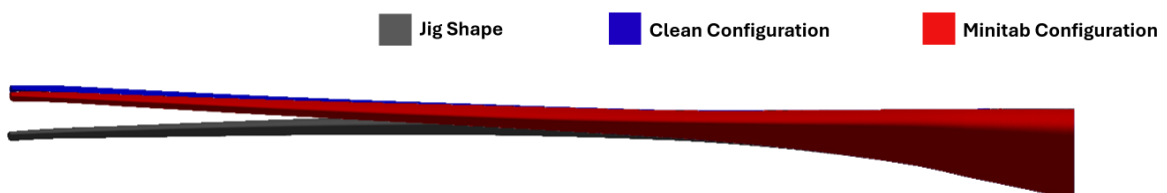
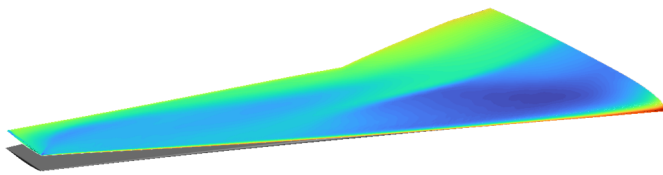
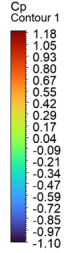


Figure 2.1: Model Wing Shapes at Steady State

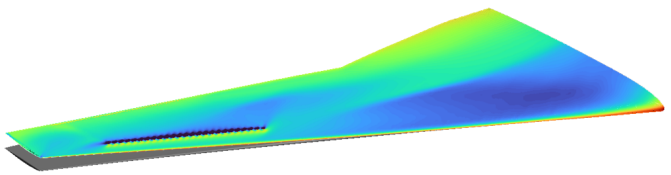
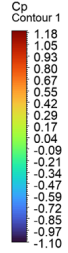
As detailed in Table 2.1, the clean wing configuration produces a lift coefficient of 0.389 and a drag

coefficient of 0.017. In comparison, the minitab wing configuration exhibits a reduced lift coefficient of 0.364 (6.42% reduction) and an increased drag coefficient of 0.021 (23.52% increase).

From the *jig shape*, the clean wing configuration exhibits an upward deflection as a result of the lift distribution generated by the wing surface along the span. For the clean wing configuration, the wing tip rises 1288.68mm from the *jig shape*. In contrast, the minitab wing configuration shows a reduced upward deflection beyond 50% of the wing span and a wing tip deflection of 1161.97mm from the *jig shape*, which is 9.8% lower than the clean wing configuration.



(a) Clean Wing Configuration



(b) Minitab Wing Configuration

Comparing the clean wing and the minitab wing pressure coefficient contours, the minitab creates a large pressure buildup on the front face followed by a region of low pressure separated flow behind it. This localized pressure differential directly contributes to the increased drag coefficient in comparison to the clean wing configuration from 0.017 to 0.021. It is important to note, the minitab's zone of influence is limited between 60-95% span of the wing and no other significant changes in the pressure distribution over the wing can be seen outside this zone.

3

Transient Simulation Plan for Minitab Wing

3.1. Methodology

A complete schematic of the FSI and CFD simulations carried out is shown in Figure 3.1. The simulations are setup first to build a base foundation with the transient aerodynamic characteristics of the minitabs, which is then followed up with the inclusion of wing flexibility in order to determine how the aeroelastic characteristics affect the performance of the minitabs.

Simulation Type	Wing Structure Type	Wing Shape	Gust	Wing Model		Purpose and Description
				Clean Wing	Minitab Wing	
CFD Transient	Rigid	Cruise Shape	✗	✗	✓	Capture pure transient aerodynamic effects of the minitabs
FSI Dynamic (Gust OFF)	Flexible	Jig Shape	✗	✓	✓	Deploying and stowing of Minitab with no gust. Compare results with baseline clean wing solution.
FSI Dynamic (Gust ON)	Flexible	Jig Shape	✓	✓	✓	Sensitivity study for deploying and stowing time, obtain a final Deploy + Stow time scheme for a gust.

Figure 3.1: Simulation Run Plan for Dynamic FSI of Minitabs

3.1.1. Case: CFD Transient

This CFD case is simulated with the transient mode enabled, which captures time dependent flow phenomena and the wing internal structure set as rigid. This set of results will provide information on the transient aerodynamic effects of the minitabs deployment of the wing alone, with no influence of the structural motion. Aerodynamic data from this case will be utilized in the dynamic FSI simulations in order to identify the sections of the wing's responses which is dominated by the aerodynamics of the deployment alone.

3.1.2. Case: FSI Dynamic (Gust OFF)

The first case of dynamic FSI simulations are conducted to evaluate the aeroelastic effects due to the deployment of the minitabs on the wing structure. These simulations are conducted with the gust input turned "OFF" in order to isolate the aeroelastic effects of the minitab deployment from excitations induced by the gust. In addition, the final wing position, shape and load distribution over the wing span are evaluated once the simulation reaches steady state.

An example representative timeline of a minitab deployment is shown in Figure 3.2. CL_1 represents the lift coefficient of the clean wing, CL_2 represents the lift coefficient of the wing with the minitab deployed.

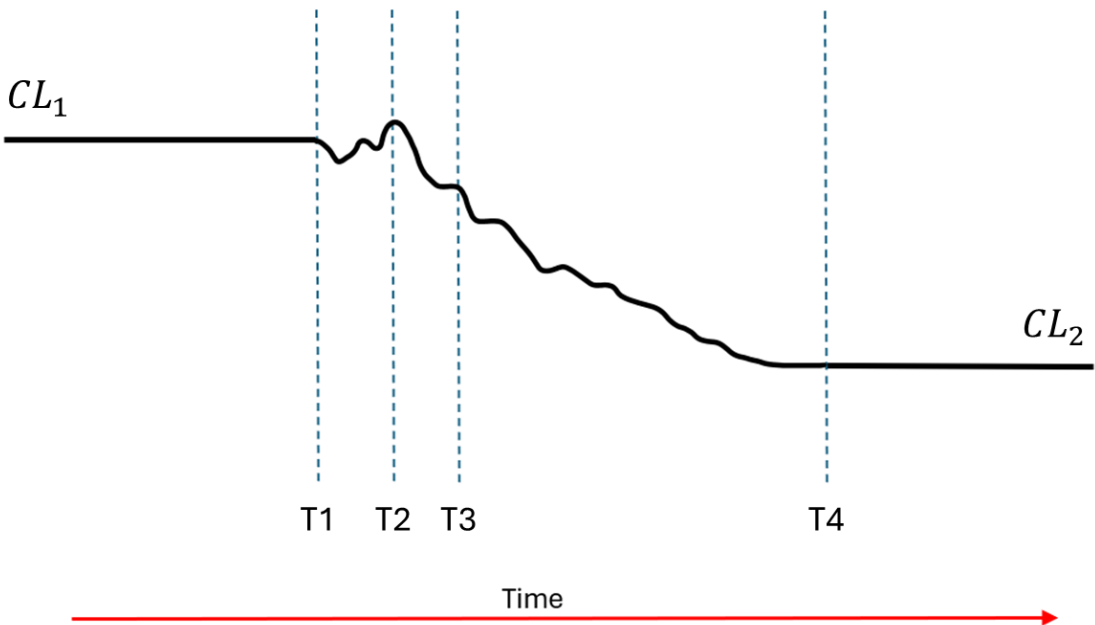


Figure 3.2: Timeline of the lift coefficient variation due to deployment of the minitabs

From Figure 3.2, 4 key points in the timeline are noted: T1 is the point when the minitabs are deployed, T2 is the point at which the peak of the gust reaches the wing, T3 is the point of conclusion of high-frequency transient phenomena in both fluid and structural responses and finally, T4 is the point at which steady state is attained following minitab deployment.

Data from this simulation is focused on capturing the transient flow characteristics and timescales during the deployment phase of the minitabs, particularly between points T1 and T3 in the timeline, with the gust disabled. Data generated for points T4 and beyond in the timeline will also show the final load distribution over the wing span, wing shape.

The midflight deployment of the minitabs during cruise conditions in absence of gusts will yield 4 important sets of data. These comprise of the transient aeroelastic deformation of the wing; the time varying load distribution over the wing surface; the transient flow characteristics, including shock formations and local flow separations during the minitab deployment period and the temporal scales of the minitabs' influence on both wing structure and the surrounding airflow.

This case will be repeated for the "**Stow Minitab**" operation as well. Similar to the minitab deployment process, the purpose of this simulation is to determine the isolated transient aeroelastic behaviour in

terms of the aerodynamics loads and structural deformations of the wing as a result of the minitab stowing.

3.1.3. Case: FSI Dynamic (Gust ON)

Once the isolated aeroelastic behaviors as a result of the minitabs deploying and stowing are determined, the next step is to introduce a discrete gust into the flow. In order to determine the influence of the minitabs in response to a gust, two sets of dynamic FSI simulations with the gust enabled are conducted: first with the clean wing configuration and the second set of simulations are with the minitab wing configuration.

The first set of results simulates the clean wing configuration subjected to various gust cases, in order to obtain a baseline of the expected aeroelastic responses in terms of magnitude and time of peak gust loads, duration of its influence and the motion of the wing structure.

Figure 3.3 illustrates a representative timeline of the lift coefficient variation for a clean wing encountering a discrete gust. In this timeline, T1 denotes the gust onset, defined as the point at which the discrete gust is at the leading edge of the wing root, and T2 is defined as the earliest point, steady state conditions is reached after the gust encounter.

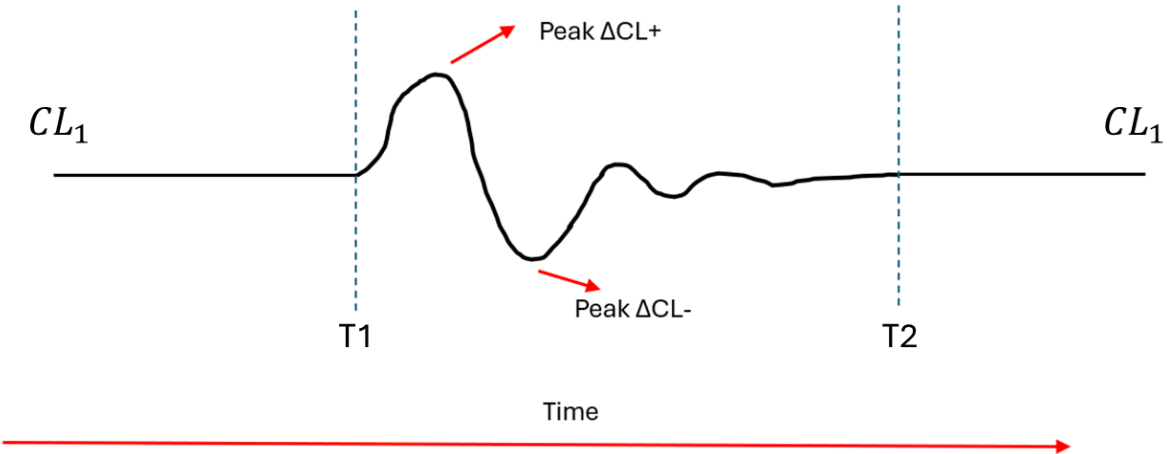


Figure 3.3: Lift Coefficient Timeline with Gust

The second set of results simulates the minitab wing configuration for the same gust cases as the clean configuration. In response to the gust, a sweep of deployment and stowing times is simulated in order to determine the appropriate times to deploy and stow the minitabs to maximize the alleviation of the peak gust loads and minimize any undesirable affects as a result of the deployment and stowing process.

A representative timeline of the variation of lift coefficient of the minitab wing configuration with the ideal deployment and stowing time in response to a discrete gust is shown in Figure 3.4.

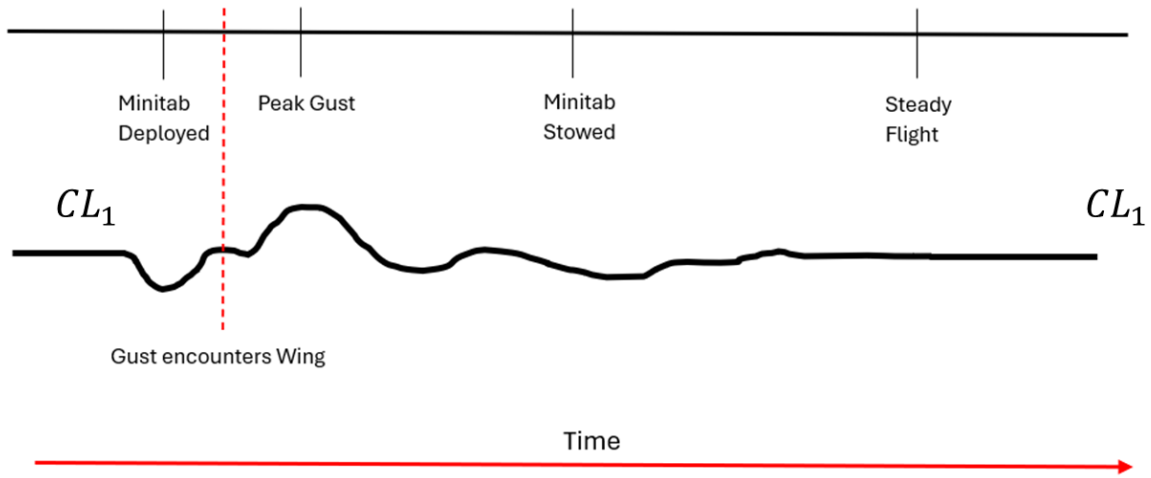


Figure 3.4: Complete Timeline of Minitab Deployment for GLA

4

Transient Results of CFD and FSI simulations

4.1. Transient CFD Results

For this case, the wing structure is set rigid in cruise shape. The minitab deployment operation is simulated under the boundary conditions as stated in Table 1.2. From Figure 4.1, the lift coefficient drops sharply after deployment to the peak minima $CL = 0.345$ in 0.2s, and finally settles to a steady state value of $CL = 0.349$.

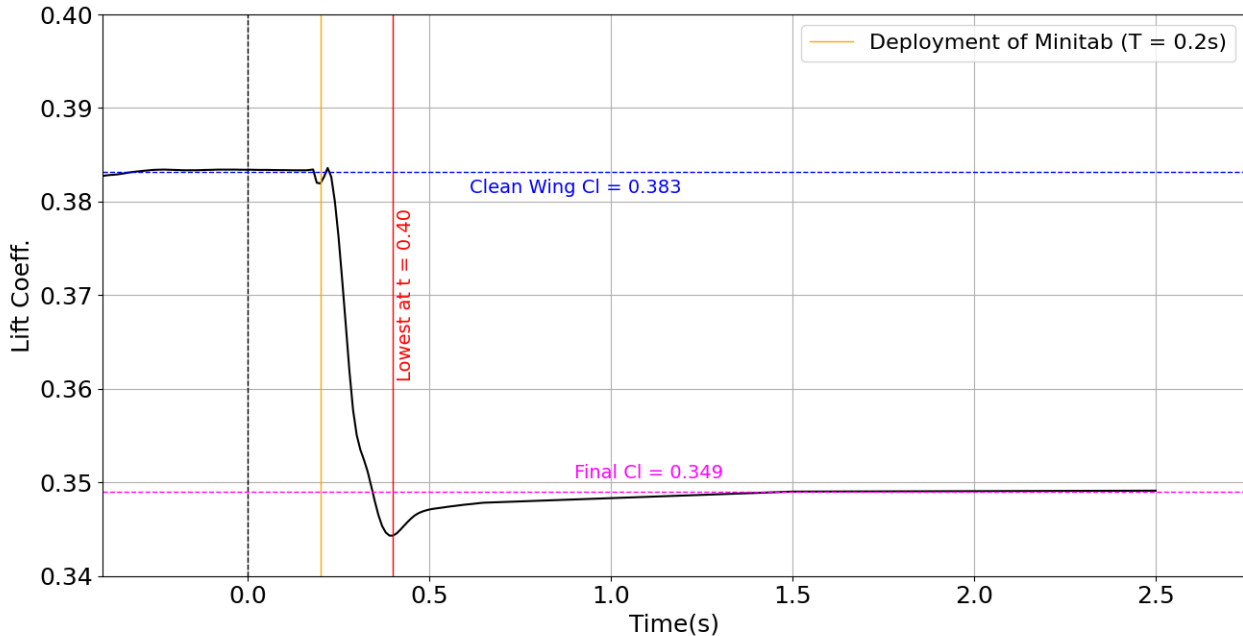


Figure 4.1: Time-dependent variation of lift coefficient during minitab deployment: CFD

At the time of deployment of the minitabs, a region of separated flow forms behind the minitabs. This region of separated flow disrupts the smooth airflow over the upper surface of the wing. Concurrently the minitabs also generate a significant pressure buildup on the front face, leading to an overall rise in pressure over the upper surface. The combination of disrupted flow downstream of the minitabs and the reduced pressure differential between the upper and lower wing surfaces ultimately results in a decreased net lift force.

4.2. Minitab Deployment Midflight with No Gust (FSI)

The first case simulated is the midflight deployment of the minitabs with no gust input. The minitab deployment was initiated at a physical time of 0.2s after steady state for the clean wing was reached. It is important to note, that the minitab is deployed and stays deployed till the end of the simulation.

4.2.1. Variation of Lift Coefficient with Time (Minitab Deployment)

From Figure 4.2, there is an immediate small drop in lift coefficient, followed by a local increase in lift coefficient in 0.04s from the baseline $CL = 0.383$ to 0.386 . Then there is a sharp drop in CL to a local minimum $CL = 0.362$ at 0.4s, which is 5.4% lower compared to the steady-state lift coefficient of the clean configuration. Once the local minimum peak is reached, the amplitude of the oscillations in the lift coefficient decays to a steady state equilibrium of $CL = 0.37$.

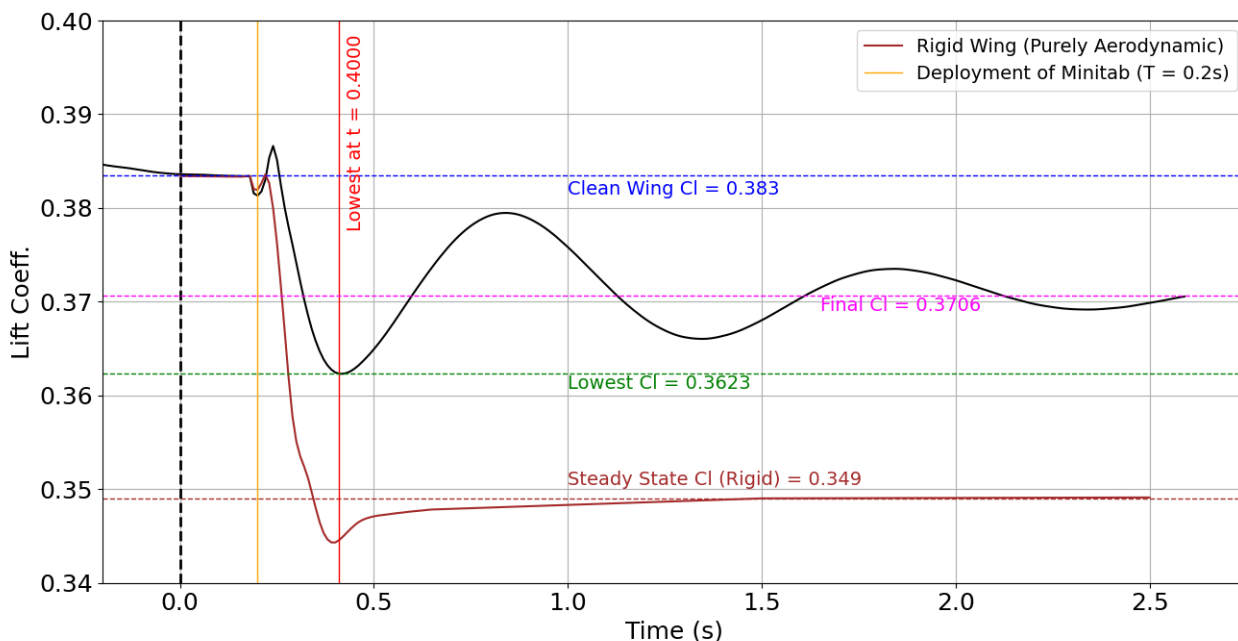


Figure 4.2: Time-dependent variation of lift coefficient during minitab deployment: FSI

The variation in lift coefficient can be split into 2 sections: variation due to the aerodynamic influence of the minitab deployment and variation due to the motion of the wing as a result of the minitab deployment. There is a notable similarity in the rapid lift reduction between the time of deployment of minitabs at 0.2s and 0.4s. This similarity suggests that the variation in the lift coefficient of the minitab configuration between the time frame of 0.2s-0.4s can be primarily attributed to the aerodynamic effects of the minitab itself.

The rapid lift reduction during this interval is characterized as "Reaction Time," denoted by the symbol T_{rea} , with a duration of 0.2 seconds.

Comparing the flexible minitab configuration and the rigid wing, the steady state lift coefficient of the rigid wing differs by 5.67%. Since the minitab configuration has a flexible structural model, the wing structure deforms and adjusts its shape to a lower upward deflection in comparison to the rigid wing. For a swept wing, a lower upward deflection increases the effective angle of attack across the wing span, resulting in higher net lift generated.

4.2.2. Variation of Wing Tip Displacement with Time (Minitab Deployment)

From Figure 4.3, at the minitab deployment occurs at 0.2 s on the timeline, there is no immediate response to the tip displacement. The wing tip begins to drop 0.15s after the minitab deployment and eventually reaches a local minimum of 1172.08mm with respect to the *jig shape*, occurring 0.65s after deployment, which is a 30.29% decrease from baseline. Once the local minima are passed, the amplitude of the oscillations decays and stabilizes to a final wingtip displacement of 1343.80mm with respect to the *jig shape*.

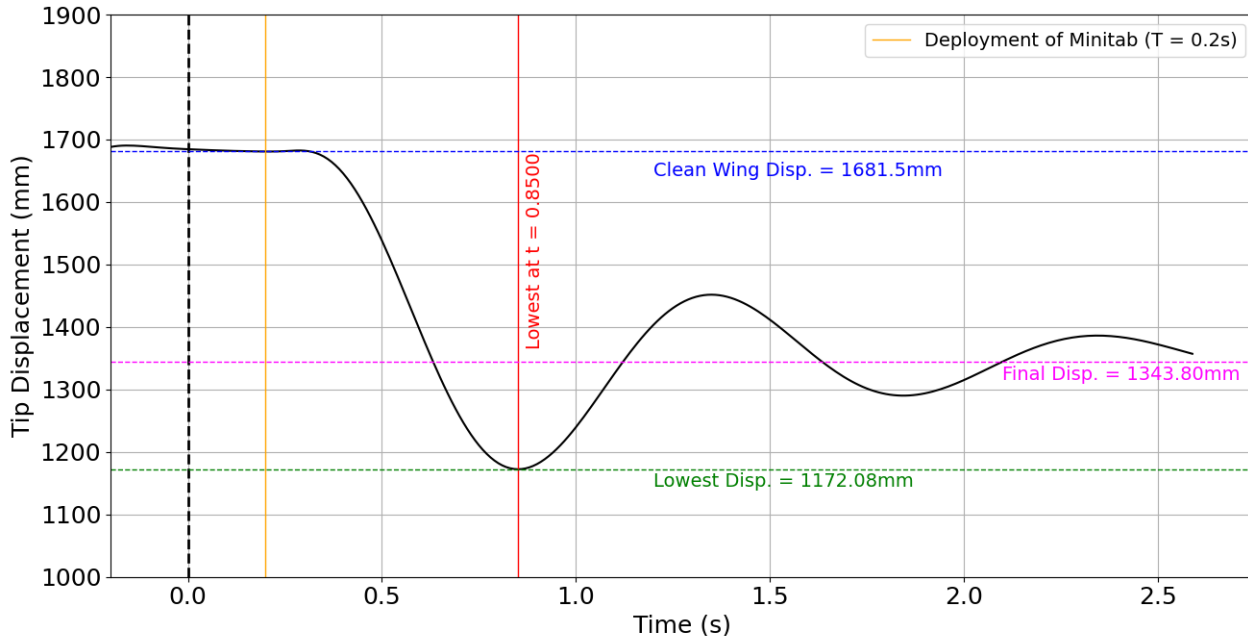


Figure 4.3: Time-dependent variation of wing tip displacement during minitab deployment: FSI

The peak minimum of the lift coefficient occurred earlier than the peak minimum of the structural tip displacement. The oscillations of the wing tip has an approximate frequency of 1Hz. The delayed response in the structural motion as a result of the change in the aerodynamic loads over the wing can be attributed to the wing's significant structural inertia and due to the fact that dynamics of a structure is governed by its eigen modes, primarily dominated by the first bending mode, which is calculated to be 0.82 Hz.

4.2.3. Spanwise Distribution of Lift Forces after Minitab Deployment

The variation of the lift forces at various spanwise locations are illustrated in Figure 4.4. The variation in the load is more pronounced in the wing span where the minitabs is installed(62% - 88% span), while spanwise sections closer to the root of the wing exhibit minimal load variations over time time.

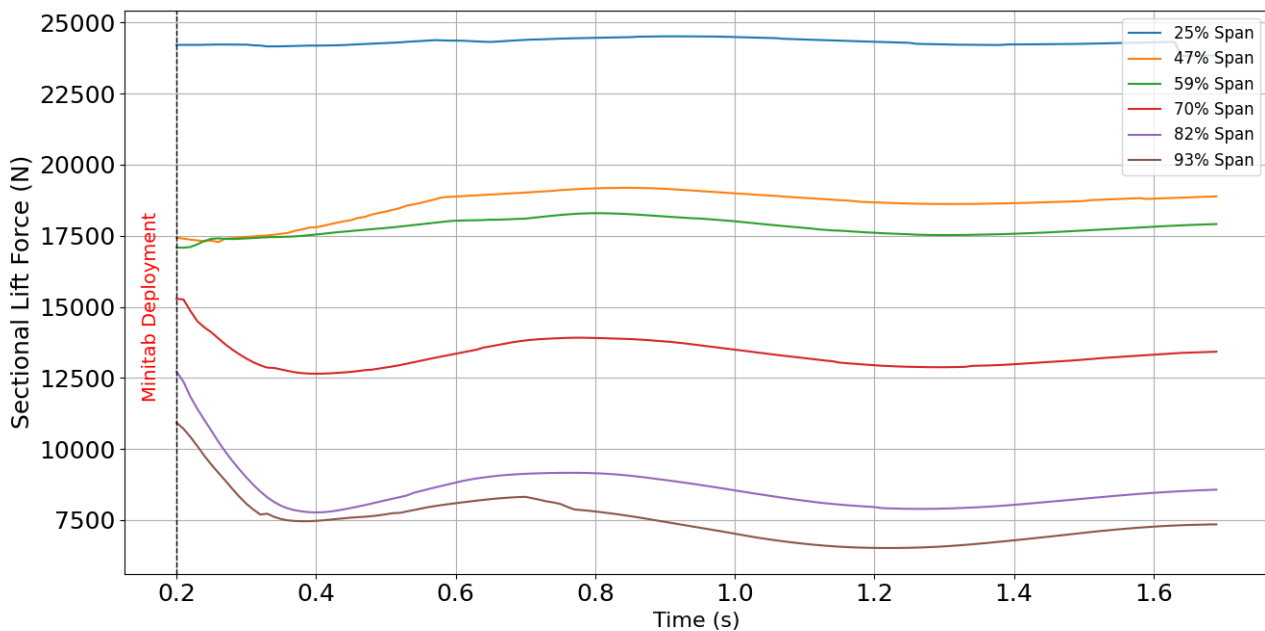


Figure 4.4: Temporal variation of sectional lift forces at multiple spanwise locations

4.2.4. Root Bending and Torsional Moments

In order to determine the internal loads of the wing structure, the root bending moment and torsion moment are plotted in Figure 4.5 and Figure 4.6 respectively.

Upon deployment of the minitabs, the root bending moment follows a trend similar to the lifting forces. The wing tip reacts to the change in the root bending moment with a delay as a result of the significant structural inertia and dominance of the first bending mode of the wing structure.

In addition, the deployment of the minitab results in an increase in the torsion moment of the wing. Since the minitabs are placed ahead of the wing's elastic axis, close to the leading edge, the additional drag force created as a result of the pressure difference across the minitab induces a positive torsional moment, which results in an increase wing twist angle.

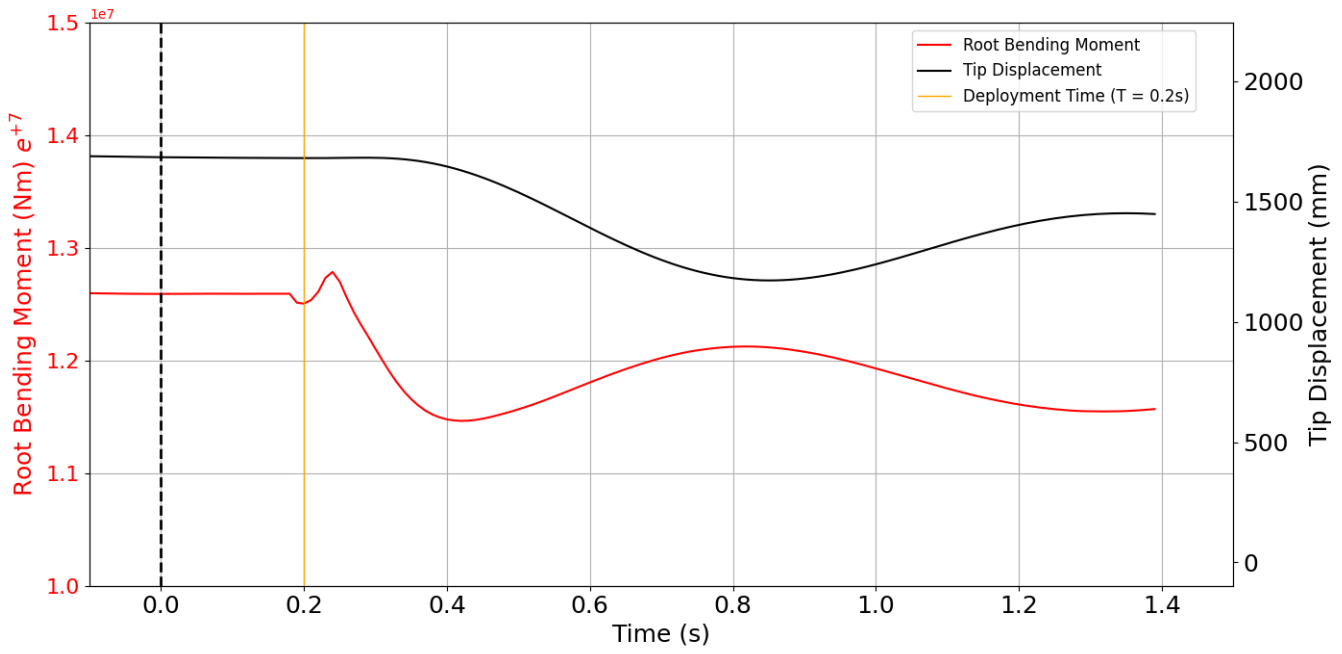


Figure 4.5: Root Bending Moment & Tip Displacement vs Time

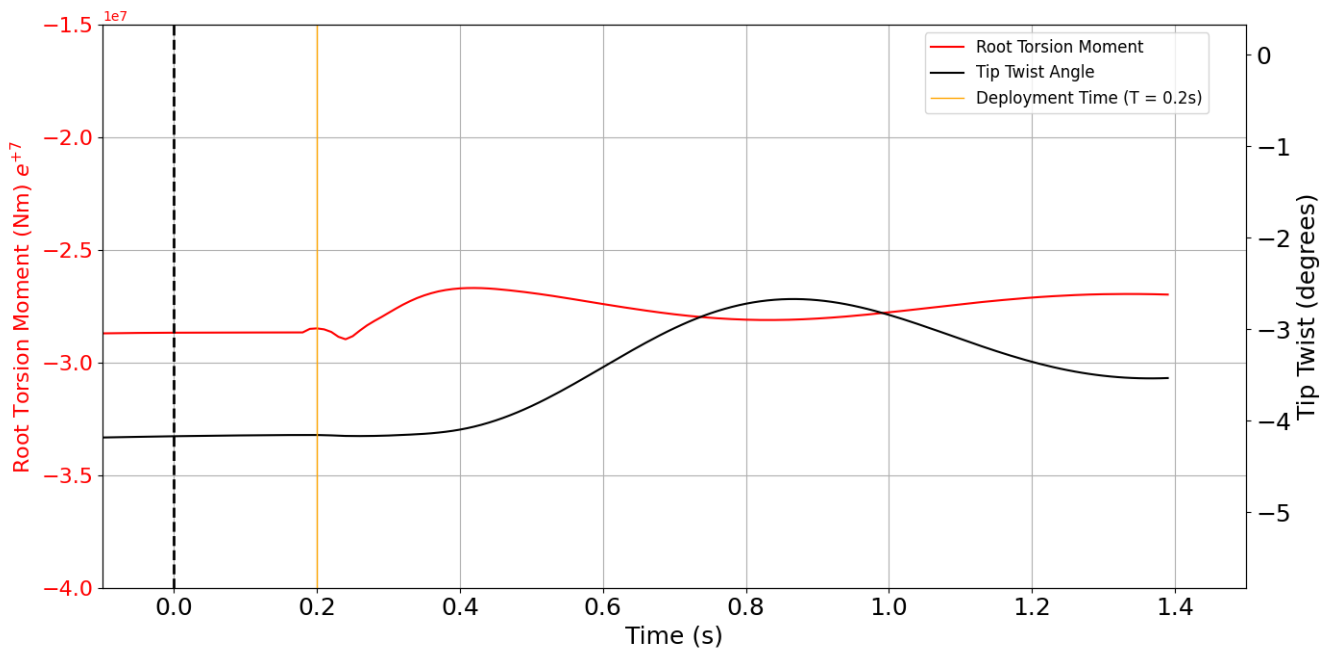


Figure 4.6: Root Torsion Moment & Tip Twist Angle vs Time

4.2.5. Influence of Minitabs on the Pressure Distribution

Pressure contours of the pressure coefficient are plotted over the upper wing surface. The range of pressure coefficient values was limited to obtain a better contrast of the contours on the surface of the wing.

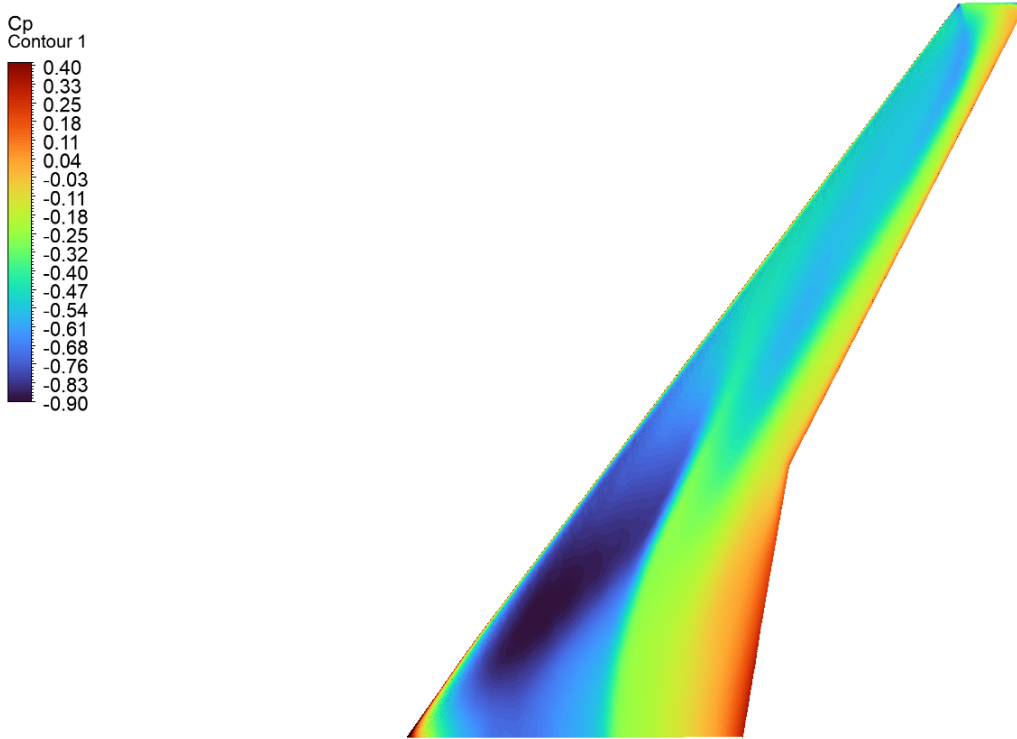


Figure 4.7: Pressure distribution over upper surface for clean configuration

Within a short time frame after deployment of the minitabs (0.04s), a region of high pressure develops in front of each of the minitabs and grows towards the leading edge, seen in Figs. 4.8(b), 4.8(c) and 4.11(a). Directly downstream of the minitab's position, small pockets of separated flow regions form, characterized by significantly lower pressures behind each minitab. These localized regions of separated flow behind each minitab coalesce in 0.04s and stabilizes for the rest of the duration of the minitab deployment.

Upon the minitab deployment and in subsequent time intervals, this normal shock over the outboard span of the wing loses its strength, while an oblique shock forms at the upper edges of the minitabs. As illustrated in Figs. 4.8(d) to 4.8(f), the pressure increases closer to the outboard minitabs, while the inboard minitabs, the pressure gradient is further aft, indicating that the shock is oriented more perpendicular to the freestream direction. This can be explained by the orientation of the minitabs parallel to the wing leading edge. The minitabs are aligned with the natural spanwise flow of a swept wing which enhances the effect on the airflow, particularly on the outboard minitabs.

On the reaction time of the minitab is passed, the shock position oscillates marginally in the chordwise direction with the oscillations of the wing structure, however no major change is noticed.

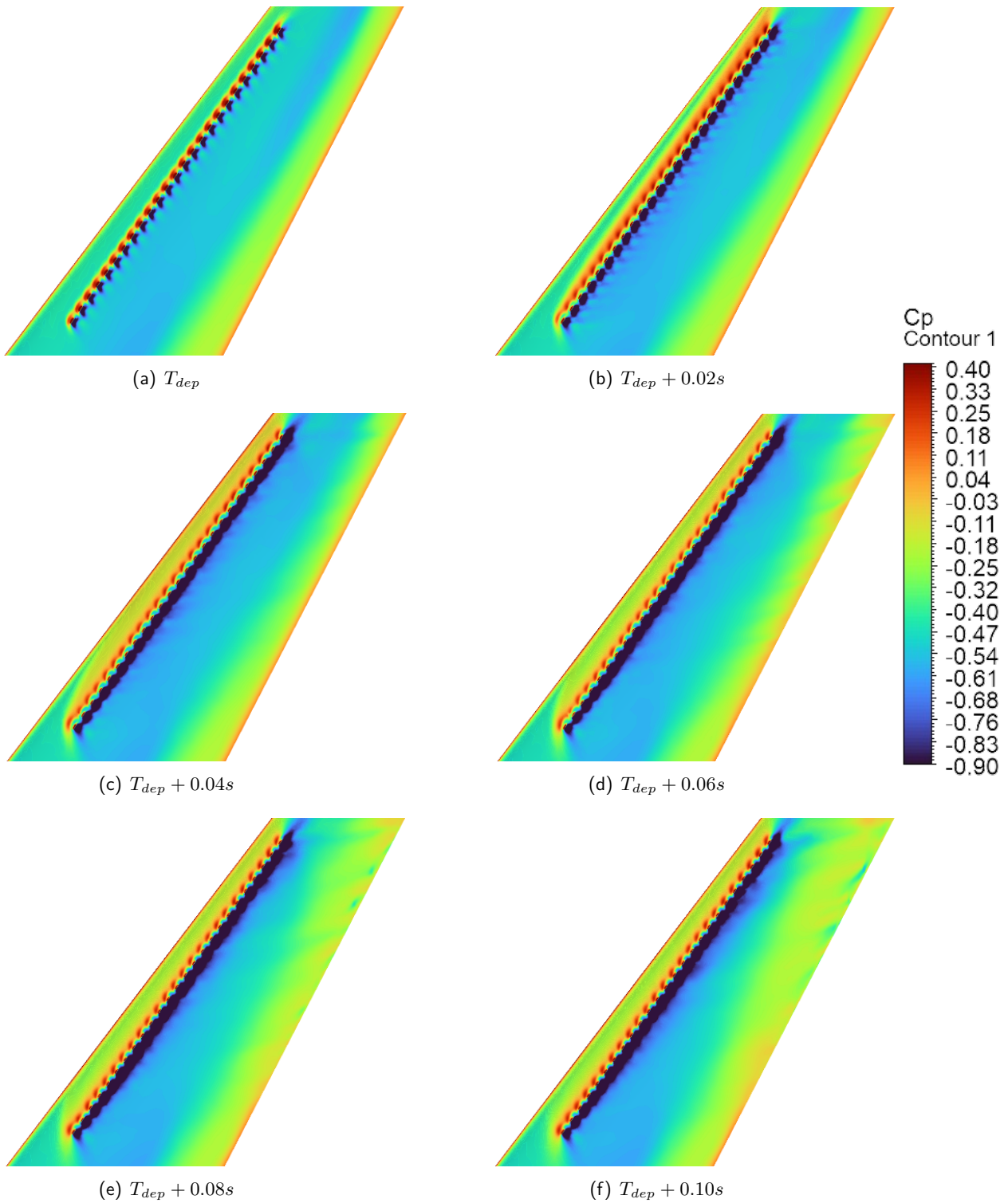


Figure 4.8: Pressure distribution at location of minitab installment

Sectional pressure coefficient is calculated at 2 spanwise locations. Figure 4.9 is plotted at the section across a minitab (75% span) and Figure 4.10 is plotted at the section in the gap between 2 minitabs (65% span).

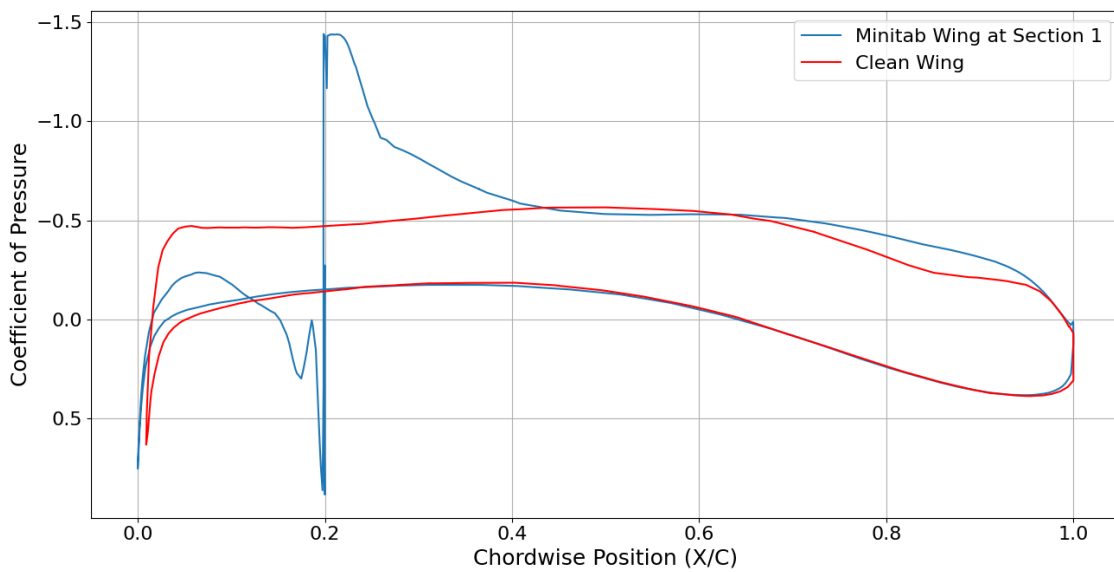


Figure 4.9: Sectional Pressure Coefficient for the clean and minitab configurations: Section 1 (75% Span)

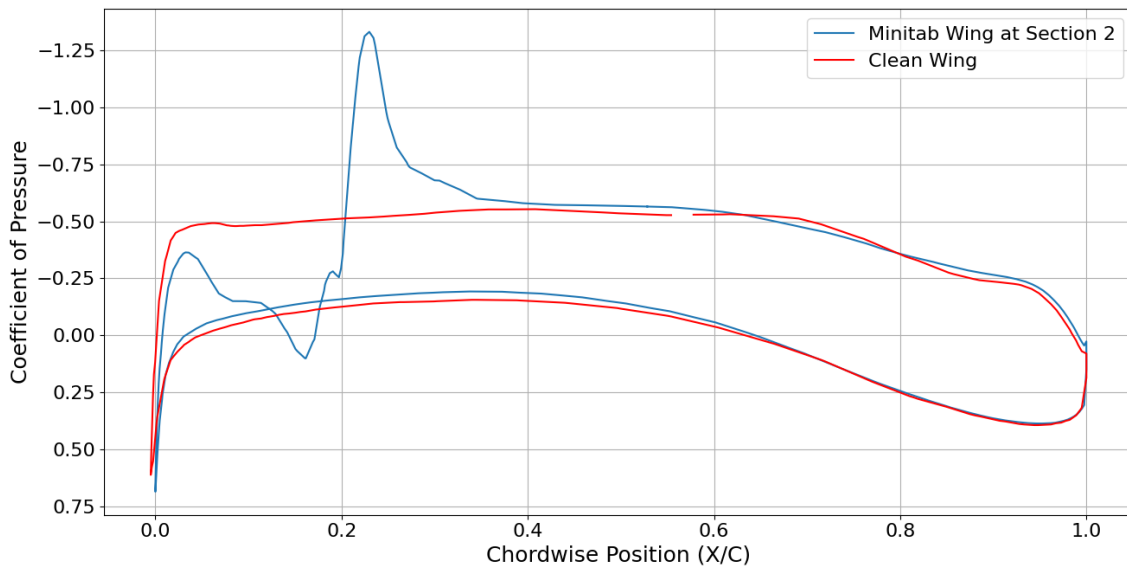


Figure 4.10: Sectional Pressure Coefficient for the clean and minitab configurations: Section 2 (65% Span)

4.2.6. Influence of the minitab on the surface flow characteristics

Analyzing the wall shear stress in the wing span of the minitabs seen in Figure 4.11 gives an indication of the direction of flow over the surface of the wing. The primary outcome from the wall shear stress is that the flow passing through the gaps between consecutive minitabs is forced into the spanwise

direction, driven towards the wing tip. In regions around the outboard minitabs, this effect is more pronounced, resulting in regions of circulating flow around the minitabs. This result corroborates the improved spanwise flow as a result of the minitab orientation over the wing.

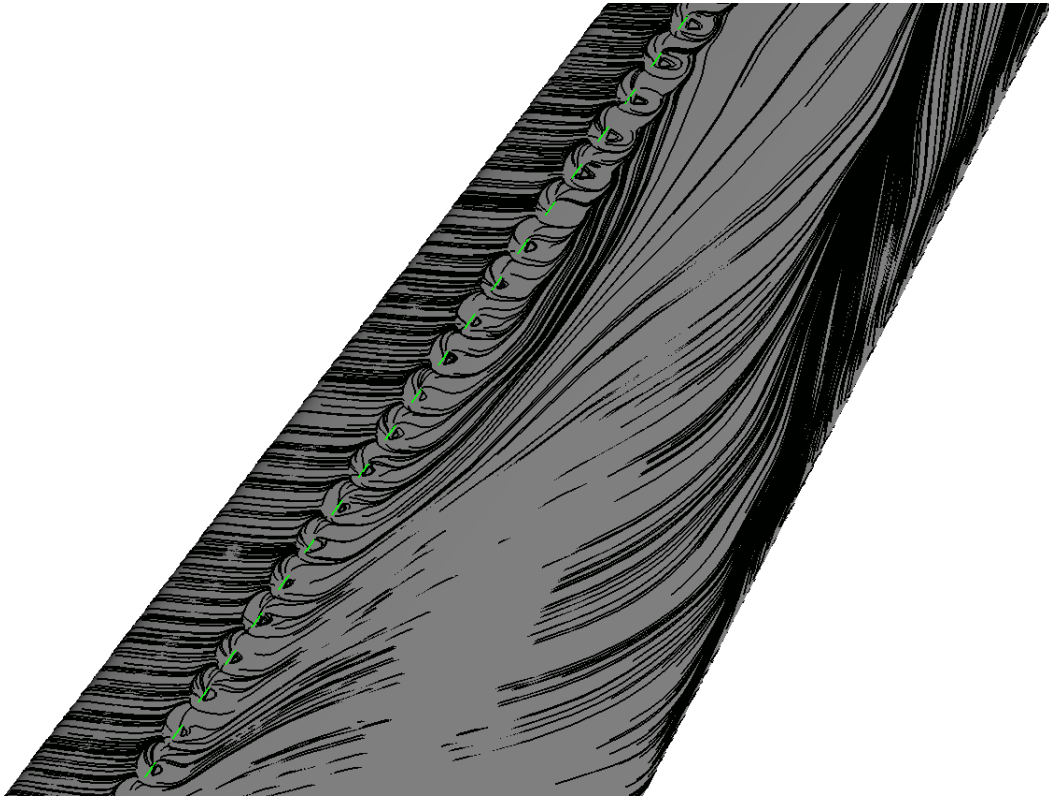


Figure 4.11: Wall Shear Stress streamlines over minitab installment location

4.3. Minitab Stowing Midflight with No Gust (FSI)

The stowing of minitabs is simulated by keeping the minitab deployed from the start till equilibrium state is reached set at $t = 0$. The minitab is simulated to be stowed by switching the boundary condition of the minitab from wall to interior flow.

4.3.1. Variation of Lift Coefficient and Tip Displacement with Time (Minitab Stowing)

From Figure 4.12, there is a small increase in CL immediately after stow in 0.03s. The CL follows a gradual dip and then begins a sharp rise to a lift coefficient local maxima of 0.394 at 0.5s ($\Delta CL = 5.84\%$). Once this peak is reached, the lift coefficient drops and oscillates in a decaying amplitude towards a steady state value of 0.383.

Applying a reasoning similar to that for the deployment of the minitabs, the initial rapid increase in lift 0.3 s after stowing is attributed to the aerodynamic effects of the minitab stowing.

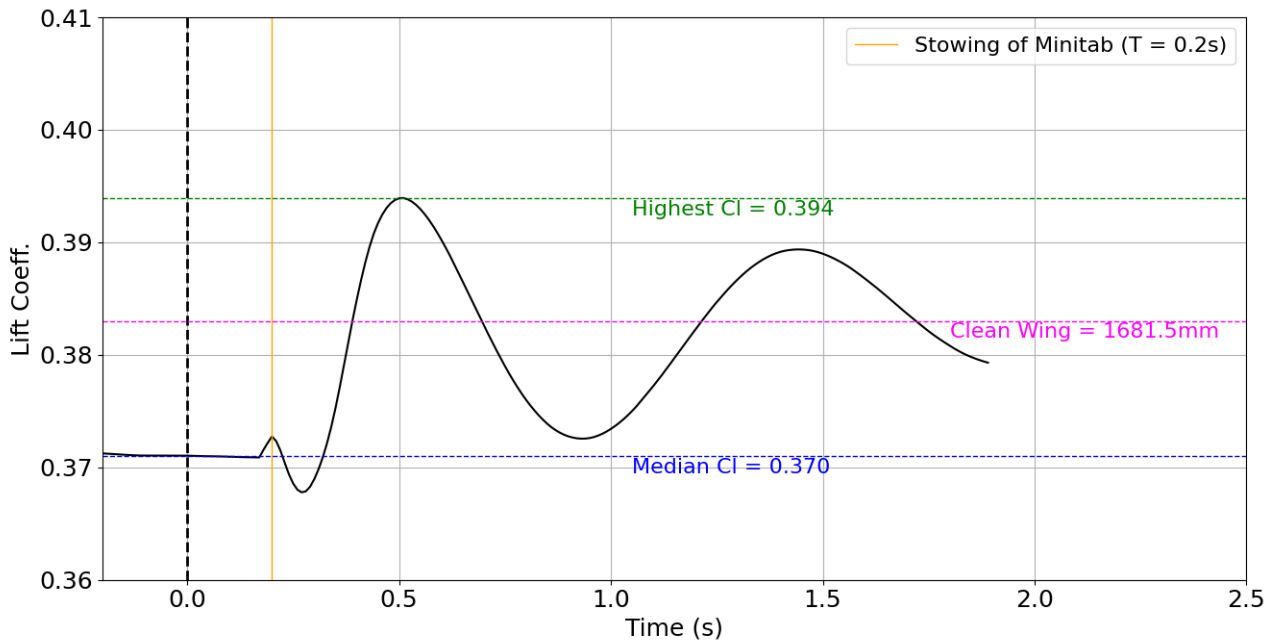


Figure 4.12: Variation of lift coefficient with time for minitab stowing

From Figure 4.13, the wing tip displacement responds with a delay of 0.25s from the time of stowing, resulting in a large wing tip deflection to 1904.04mm, 42% higher from the steady state wing tip displacement prior to stowing the minitabs. Passing this peak, the wing tip oscillates with a decaying amplitude towards a median wing tip displacement of 1681.5mm, corresponding to the clean configuration.

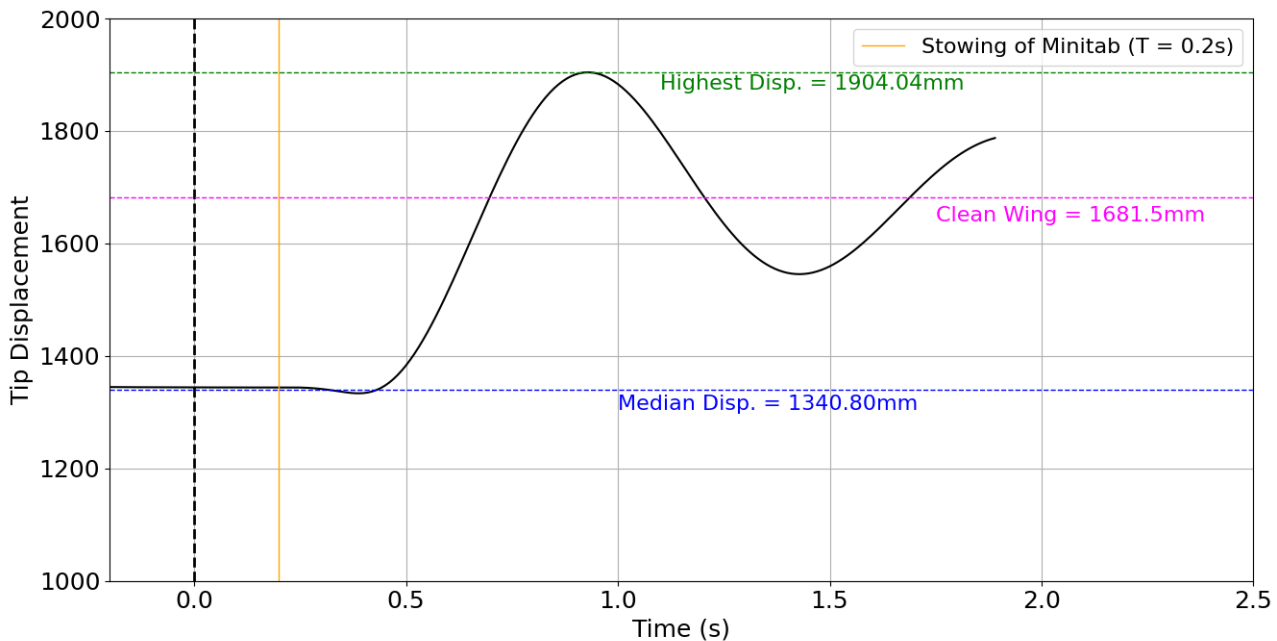


Figure 4.13: Variation of tip displacement with time for minitab stowing

4.4. Clean Configuration with Various Gust Profiles (FSI)

In order to determine the load alleviating capabilities of minitabs, we require baseline data of the responses of a clean wing encountering various gust profiles.

Table 4.1: Gust Profiles

Gust	Gust Amplitude (m/s)	Gust Length/Gradient (m)
G1	6.808	10
G2	7.473	17.5
G3	7.931	25
G4	8.902	50

4.4.1. Peak Lift Coefficient and Recovery Time for Various Gust Profiles

Figure 4.14 plots the variation in the lift coefficient in response to the chosen gust profiles stated in Table 4.1 for the clean configuration.

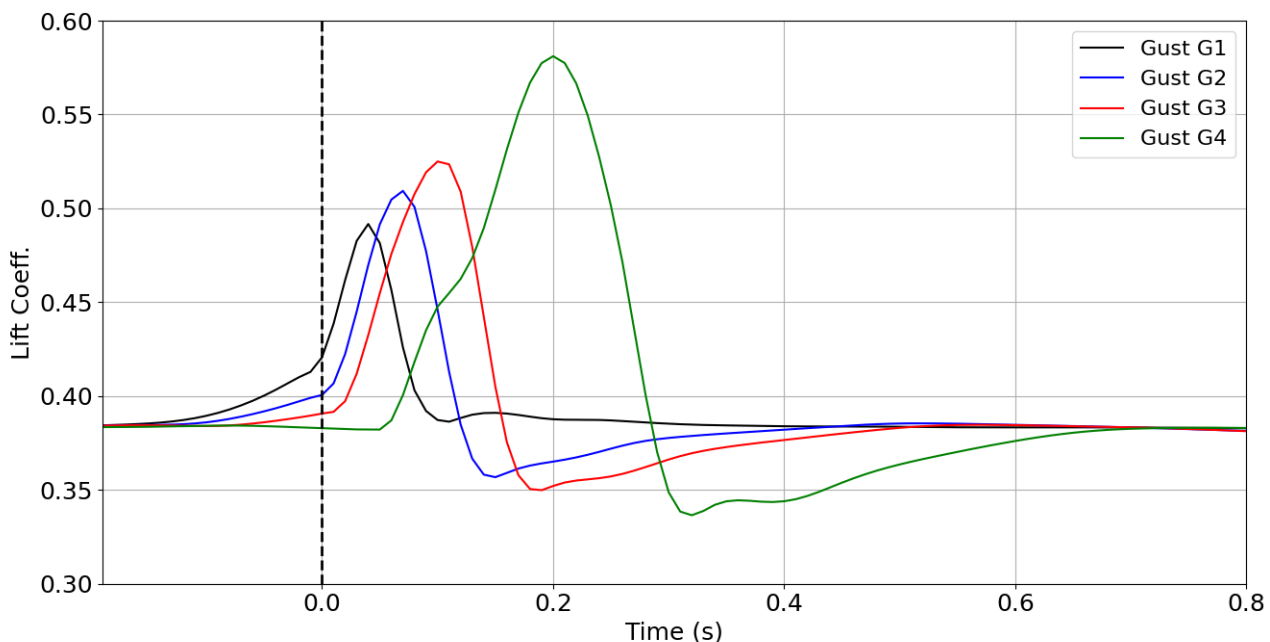


Figure 4.14: Variation of lift coefficient for all gust profiles in clean configuration

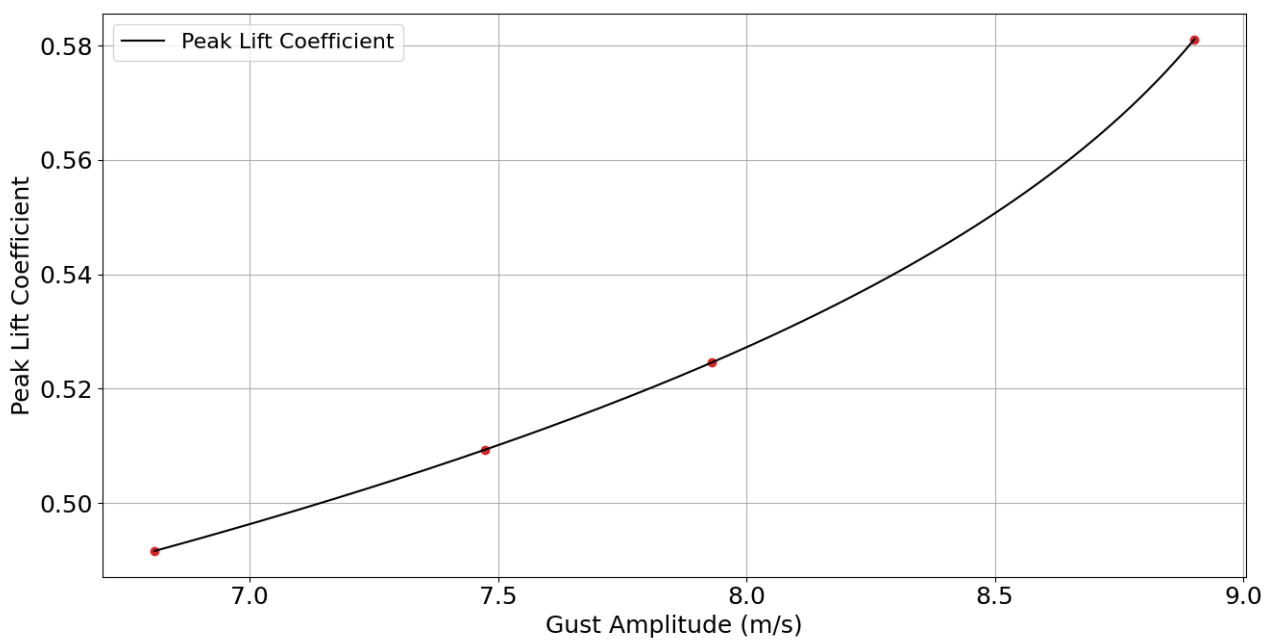


Figure 4.15: Variation of peak lift coefficient with gust length (m)

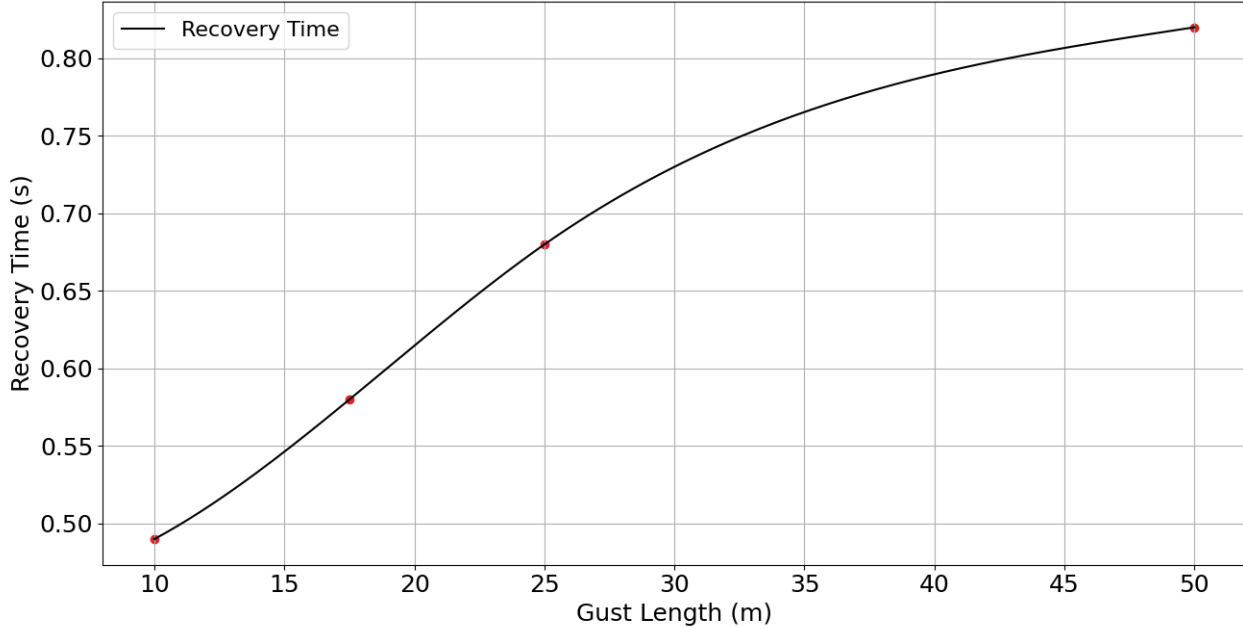


Figure 4.16: Effect of gust length on the recovery time(T_{rec})

4.5. Minitab Deployment Midflight with Gust (FSI)

With the aeroelastic results of the midflight deployment of the minitabs and a reaction time T_{rea} of 0.2s determined, the next step is to include gusts in order to determine the gust load alleviation capability of the minitabs. The minitabs will be deployed at various moments across the gust timeline, to determine an ideal time of deployment to maximize the alleviation of the gust loads.

To standardize the range of deployment times, a non-dimensional parameter known as the Deploy Time Ratio (DTR) will be utilized, evaluated by Equation 4.1. The Deploy Time Ratio (DTR) is defined as the sum of the time taken for minitab deployment (T_{dep}) and the reaction time (T_{rea}), divided by the time required for the gust to traverse its length in the freestream direction. Mathematically, it can be expressed by the Equation 4.1:

$$DTR = \frac{[T_{dep} + T_{rea}]}{\left[\frac{H}{U_\infty}\right]} \quad (4.1)$$

where T_{dep} is time of minitab deployment, T_{rea} is the minitab reaction time, H is the gust length and U_∞ is the freestream velocity. This dimensionless parameter evaluates the relation between the dynamics of the minitabs with the timescales of gust encounters.

For each gust case, 4 deployment times are chosen such that there is always an overlap between the time period of the gust peak perturbation and the minitab's reaction time interval.

Gust Profile	Time of Gust Peak	Time of Deployment	DTR
G1	0.04s	-0.36s	-4.00
		-0.26s	-1.50
		-0.16s	1.00
		-0.06s	3.50
G2	0.07s	-0.33s	-1.92
		-0.23s	-0.46
		-0.13s	1.00
		-0.03s	2.46
G3	0.10s	-0.31s	-1.09
		-0.20s	-0.04
		-0.10s	1.00
		0.00s	2.04
G4	0.20s	-0.22s	-0.12
		-0.11s	0.44
		0.00s	1.00
		0.11s	1.56

4.5.1. Gust Case G1: Variation with Deploy Time Ratio (DTR)

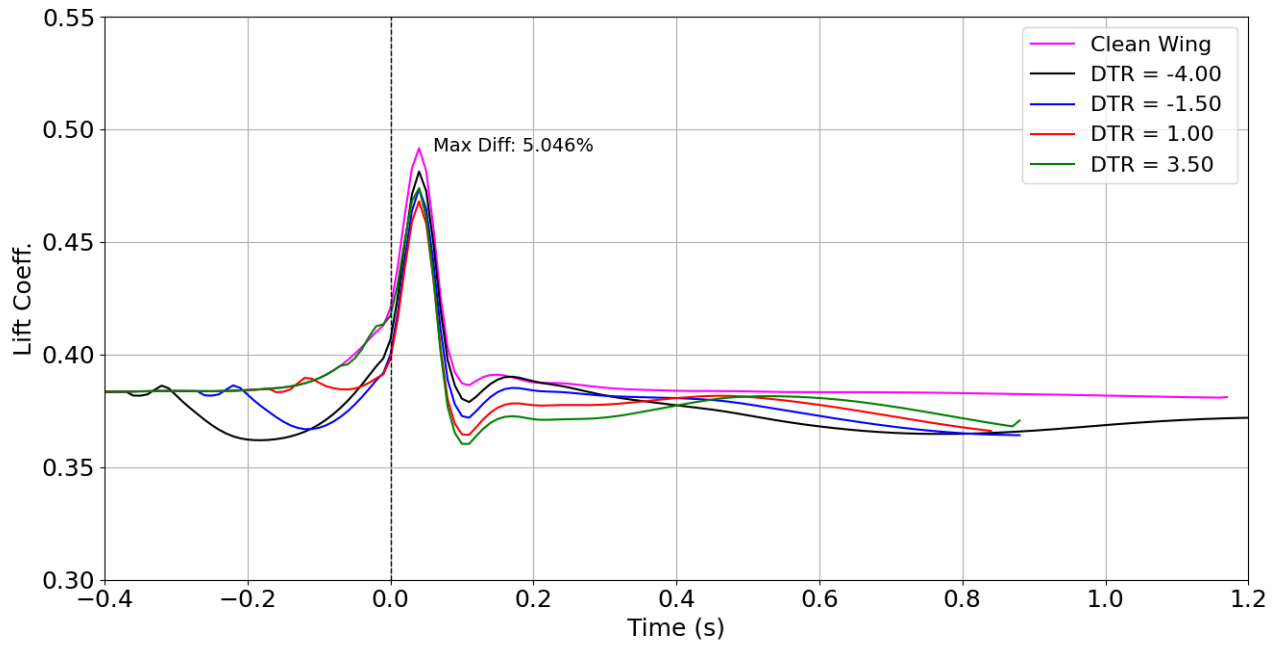


Figure 4.17: Gust G1: Lift coefficient variation for different DTR values

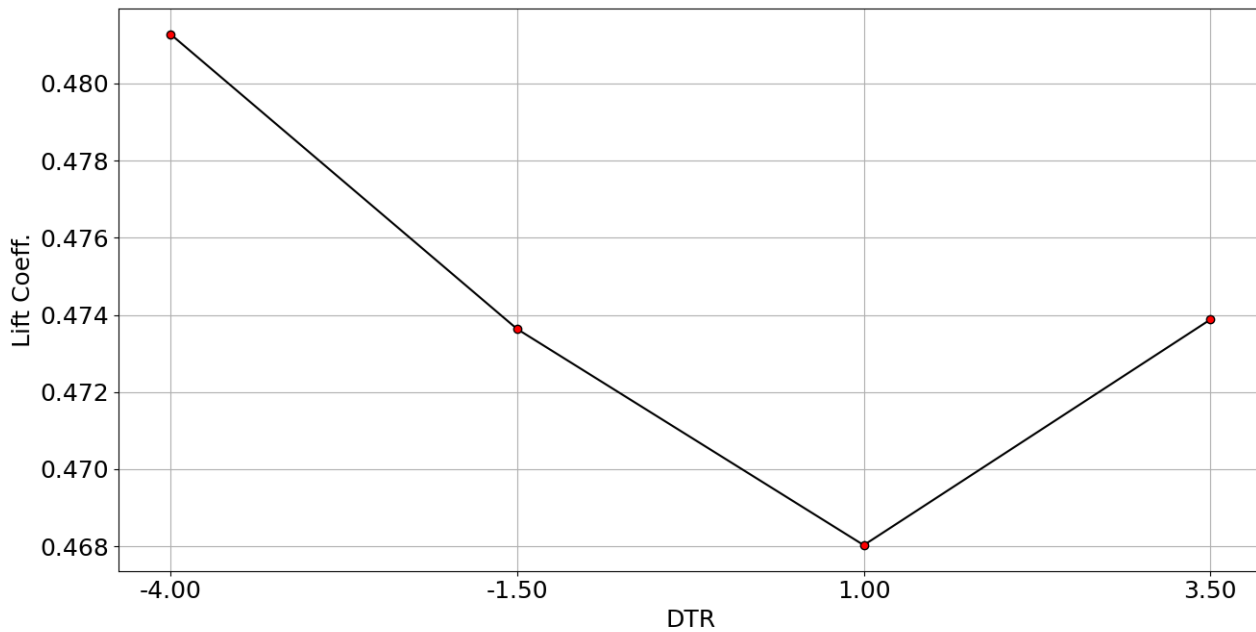


Figure 4.18: Lift Coefficient at Gust Peak (G1) vs DTR Configurations

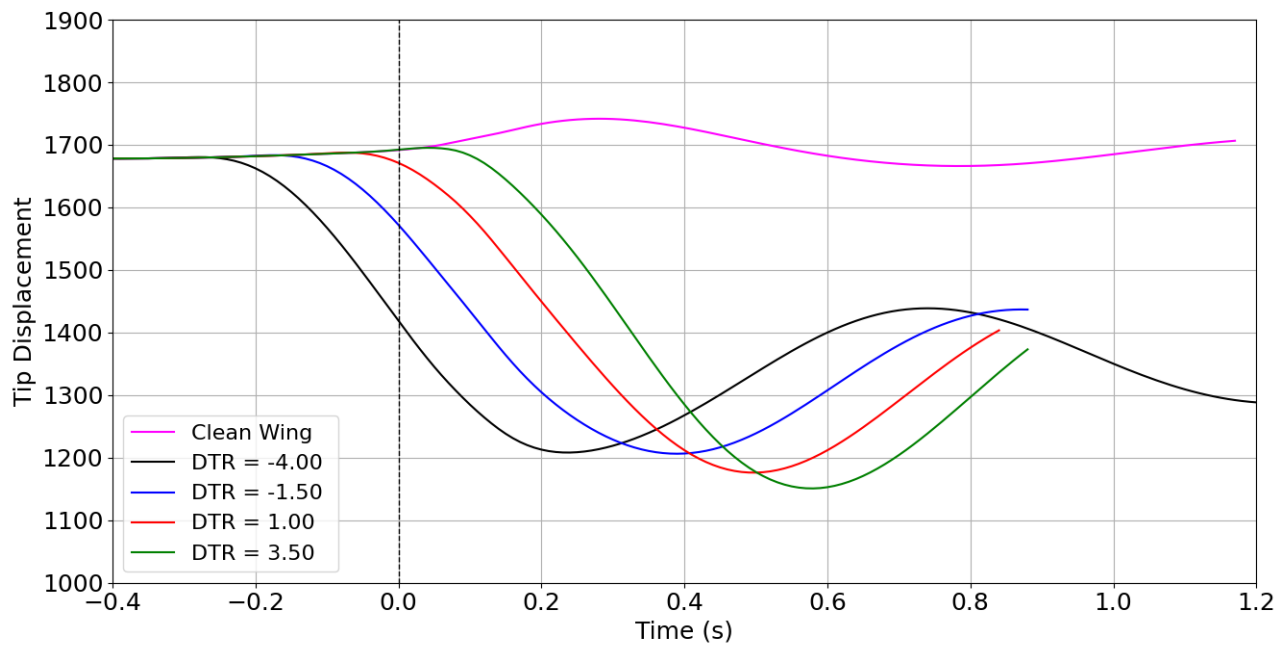


Figure 4.19: Gust G1: Wing tip displacement variation for DTR values

4.5.2. Gust Case G4: Variation with Deploy Time Ratio (DTR)

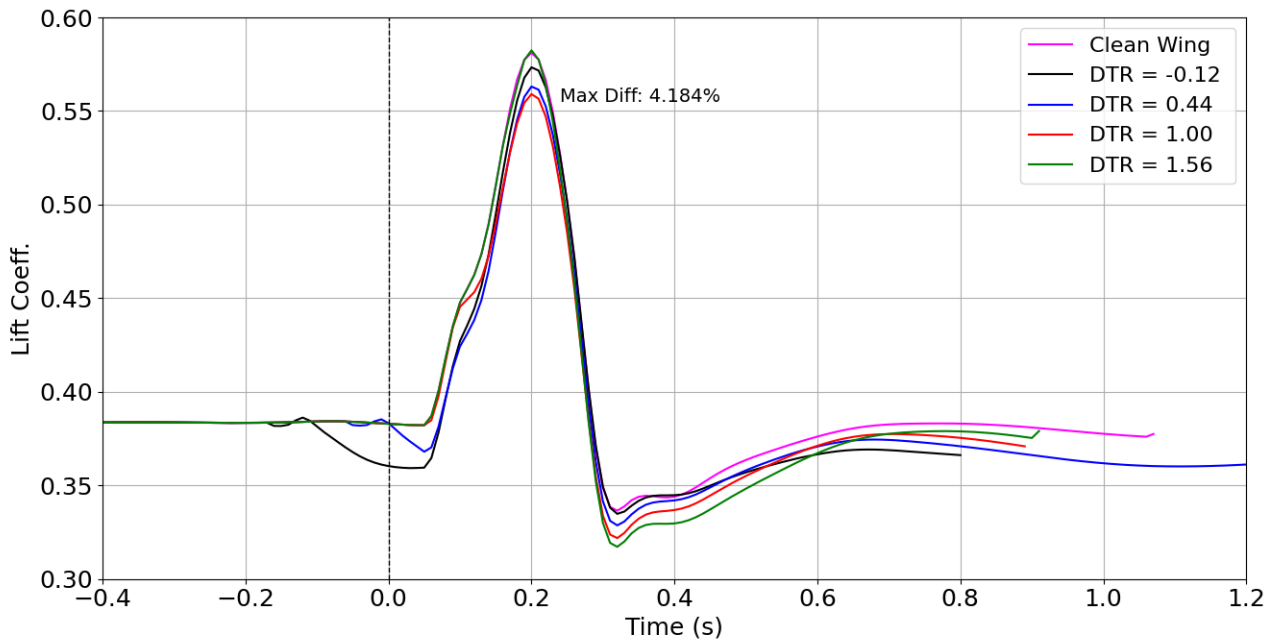


Figure 4.20: Gust G4: Lift coefficient variation for different DTR values

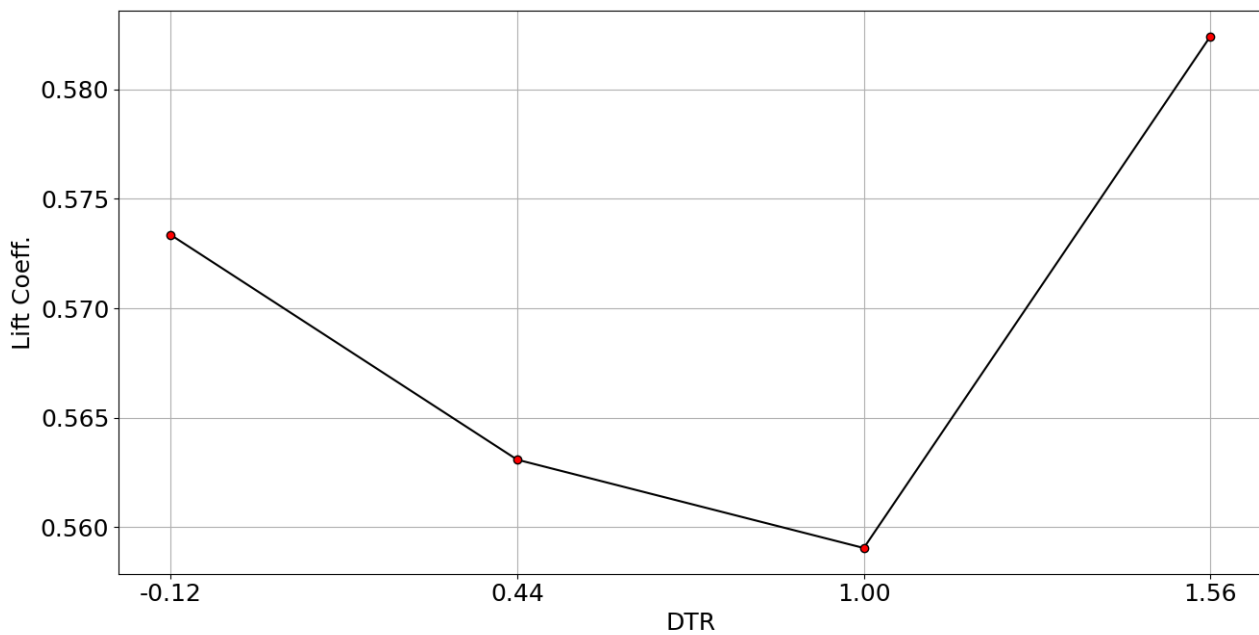


Figure 4.21: Lift Coefficient at Gust Peak (G4) vs DTR Configurations

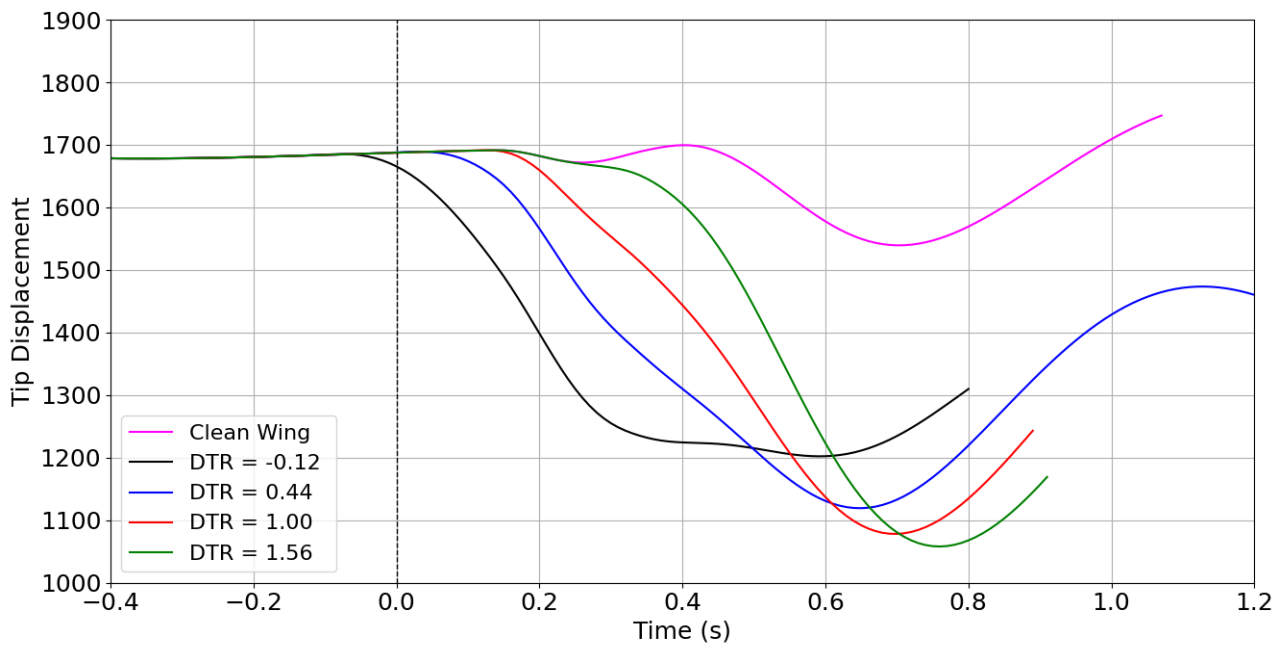


Figure 4.22: Gust G4: Wing tip displacement variation for different DTR values

Note that the results of the gust cases G1 and G4 are shown in this section, and results of gust cases G2 and G3 are plotted in Section A.3.